Repeatable Perovskite Solar Cells Through Fully Automated Spin-Coating and Quenching

Daniel O. Baumann,[*,†] Felix Laufer,[†,‡] Julie Roger,[†] Roja Singh,[†,‡] Mohammad Gholipoor,[†] and Ulrich W. Paetzold[*,†,‡]

†*Institute of Microstructure Technology (IMT), Karlsruhe Institute of Technology, 76344 Eggenstein-Leopoldshafen, Germany*

‡*Light Technology Institute (LTI), Karlsruhe Institute of Technology, 76131 Karlsruhe, Germany*

E-mail: daniel.baumann4@kit.edu; ulrich.paetzold@kit.edu

Abstract

Enhancing reproducibility, repeatability, as well as facilitating transferability between laboratories will accelerate the progress in many material domains, wherein perovskite-based optoelectronics are a prime use case. This study presents fully automated perovskite thin film processing using a commercial spin-coating robot in an inert atmosphere. We successfully apply this novel processing method for the first time to anti-solvent quenching. This process is typically difficult to reproduce and transfer and is now enhanced to exceptional repeatability in comparison to manual processing. Champion perovskite solar cells demonstrate power conversion efficiencies as high as 19.9 %, proving the transferability of established manual spin-coating processes to automatic setups. Comparison with human experts reveals that the performance is already on par, while automated processing yields improved homogeneity across the substrate surface. This work demonstrates that fully automated perovskite thin film processing

improves repeatability. Such systems bear the potential to become a foundation for autonomous optimization and greatly improve transferability between laboratories.

Keywords

Automated, robotic, repeatable, reproducible, spin-coating, perovskite, solar cells, photovoltaic

Introduction

While the power conversion efficiency (PCE) of perovskite solar cells (PSC) has steadily increased over the past years, a major disparity between the performance of champion devices and the majority of solar cells persists (see SI: Figure S1). Spin-coating is the most widespread method of depositing these perovskite thin films, dominating with record PCEs above 26 %. However, the process faces limited repeatability and reproducibility due to very narrow process windows, high dependency on precursor quality, and sensitivity to crystallization parameters which are crucially influenced by manual human processing.[1] Repeatability and reproducibility are often imprecisely used synonymously, but their meanings are slightly different.[2] In this work, we focus on repeatability, meaning obtaining the same or consistent results when an experiment is redone (repeated) under perfectly identical conditions. Reproducibility, in contrast, means obtaining consistent results under as similar as possible conditions as the original experiment (e.g., using the same methodology), but with different surroundings or operator.[2,3] While these terms are well distinguished in scientific literature,[2,3] they are not always consistently used. Reproducing the solvent quenching step in perovskite thin film processing presents a significant challenge, even within the same lab, especially when tools like pipettes or spin-coaters are not perfectly identical.[4] The processing environment, especially the solvent atmosphere, plays a crucial role in the crystallization process.[5,6] While introducing an external solvent atmosphere during annealing can sometimes

be beneficial,[6,7] an uncontrolled atmosphere can lead to reduced repeatability and transferability of perovskite thin films.[4,8] Therefore, precise control of processing conditions and the environment is essential to enable the transfer of recipes between research groups to build on each other's findings and advance the field. Recent advances demonstrate the promise of high throughput, automated experimentation and machine learning (ML) for accelerating materials discovery and optimizing material processing. Some acceleration platforms focus on discovering novel material combinations via screening methods and ML approaches,[8–17] while others investigate stability using high throughput methods.[18–23] Learning and optimization algorithms can reduce the required number of experiments[24–28] and can also accelerate process optimizations.[29–32] Other studies test mobile autonomous robots to replace the human experimenter.[33–35] All such approaches are based on the assumption that automated processing produces consistent and comparable experimental findings. However, no clear evidence for the high repeatability of automated perovskite thin film fabrication has been presented yet. In response, our research tests this assumption for perovskite thin film fabrication using a fully automated spin-coating setup. Expanding on established findings, we publish for the first time a detailed evaluation of repeatability regarding four aspects: Firstly, performance is compared across nine batches of PSCs with automatically fabricated thin films. Furthermore, we compare the perovskite thin films with regard to their structural, compositional, and optoelectronic properties. Secondly, we present our champion PSC showing the transferability of an established triple cation 1.59 eV perovskite composition to the automated fabrication. Thirdly, the device performances are contrasted with reference devices processed by experienced human experimenters. Finally, differences in homogeneity are similarly contrasted. All of this is the first publication to apply the complex one-step anti-solvent quenching method using automated processing within an inert glovebox.

To automatically fabricate the perovskite thin films we used a fully automated spin-coating robot (shown in Figure 1a). It autonomously performs sample positioning, pipetting, timed anti-solvent dispensing, and annealing processes. The robot gripper has four degrees

of freedom and interacts with objects on the base platform of $150 \times 75 \times 50$ cm^3. The gripper handles the glass substrates and places them in the spin-coater, on the hotplates, and in the substrate parking positions. The liquid handling system fills a pipette tip with the solution and dispenses it on the substrate positioned in the spin-coater. Precise timing and control of anti-solvent dispensing is performed using a syringe pump. The fully automated robotic setup was acquired from Sciprios GmbH. The system operates in a controlled N_2 glovebox with constant circulation and filtering helping to mitigate variations in the solvent atmosphere. The glovebox is equipped with an active charcoal filter for non-polar solvents and a regeneratable molecular sieve for polar solvents. Additional measures, such as continuous removal of solvent vapours via a small pump, and regular replacement of absorbing tissues, are applied to further control the local atmosphere during crystallization, reducing variability.

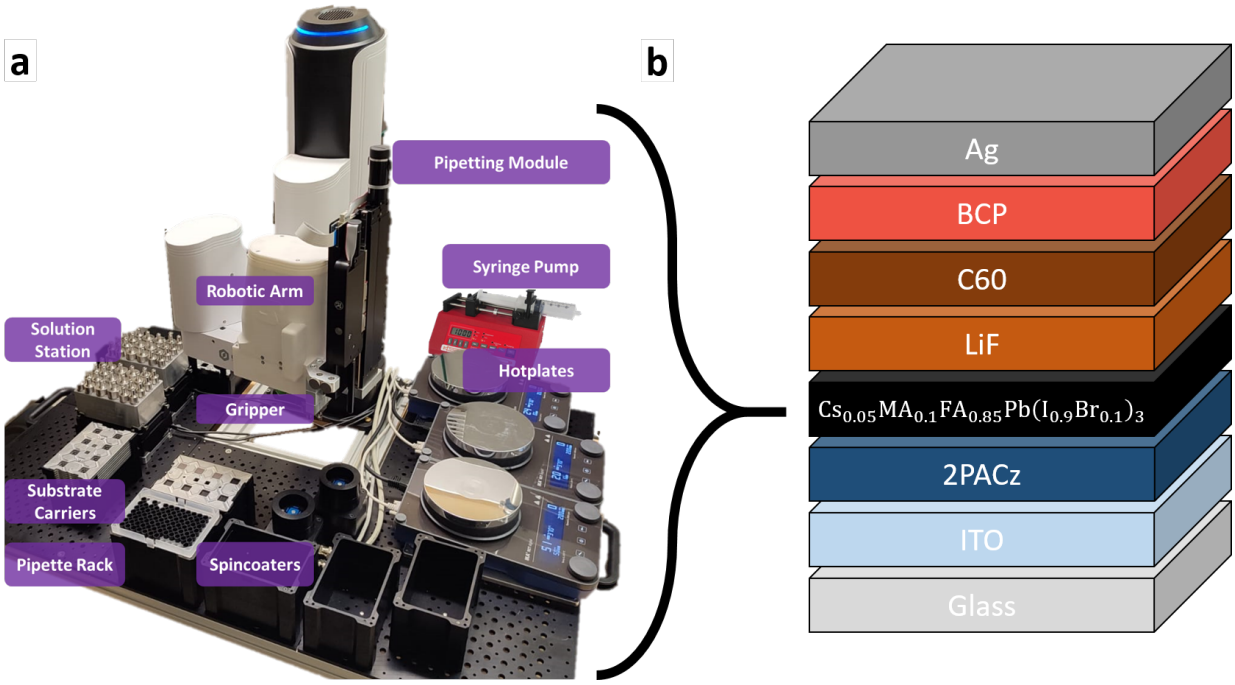

Figure 1: a) Fully automated spin-coating robot used for fabricating perovskite thin films. It is fully integrated into a N_2 filled glovebox. b) Architecture of the perovskite solar cell devices.

The p-i-n architecture for the devices consists of a Glass-ITO-2PACz-Perovskite-LiF-

C60-BCP-Ag layer stack. The perovskite absorber layer is a $Cs_{0.05}MA_{0.1}FA_{0.85}Pb(I_{0.9}Br_{0.1})_3$ composition with a 1.59 eV bandgap energy. This perovskite has previously been used to realize two-terminal tandem solar cells in our research group,[36] and similar triple cation Cs-MA-FA perovskite compositions have been intensively studied in recent years.[1,37,38] Experimental Methods provides a detailed description of the fabrication procedure and precursor composition.

Results and Discussion

Repeatability: To become a feasible alternative to manual spin-coating, automated spin-coating of perovskite thin films must first prove excellent repeatability. Repeatability means consistent performance as well as uniform structural, compositional, and optoelectronic properties across devices. We present evidence that automatic spin-coating produces highly repeatable results across nine batches (see Figure 2) in terms of high device performance (a), optoelectronic properties (b), as well as structural and compositional properties (c):

(a) Device performance repeatability is demonstrated both by the median device PCE surpassing 17 % as well as the champion device PCE surpassing 18 % in all nine batches. Within each batch, PCE standard deviations (σ_i) are low, as is the median variation across batches ($\sigma_{medians} < 0.4$ %), and total variation across all PSCs ($\sigma_{all} < 1$ %). The coefficient of variation (CV) σ/μ for the device performance across all cells is 0.053. The average yield of functioning devices across all batches is 82 %, where a functioning device is defined by fill factor (FF) > 65 % and $V_{oc} > 0.9$ V (For all devices, ranges and other JV-Parameters see Figure S4 and Figure S3). This yield appears lower than expected, but it was evaluated very conservatively and includes also losses induced from surrounding processes, mechanical handling problems of the spin-coater, and software fails requiring manual interruption and restart. Overall, directly comparing the PCE variability in this experiment with previous studies proves difficult. In the perovskite literature, discussions are typically centered around

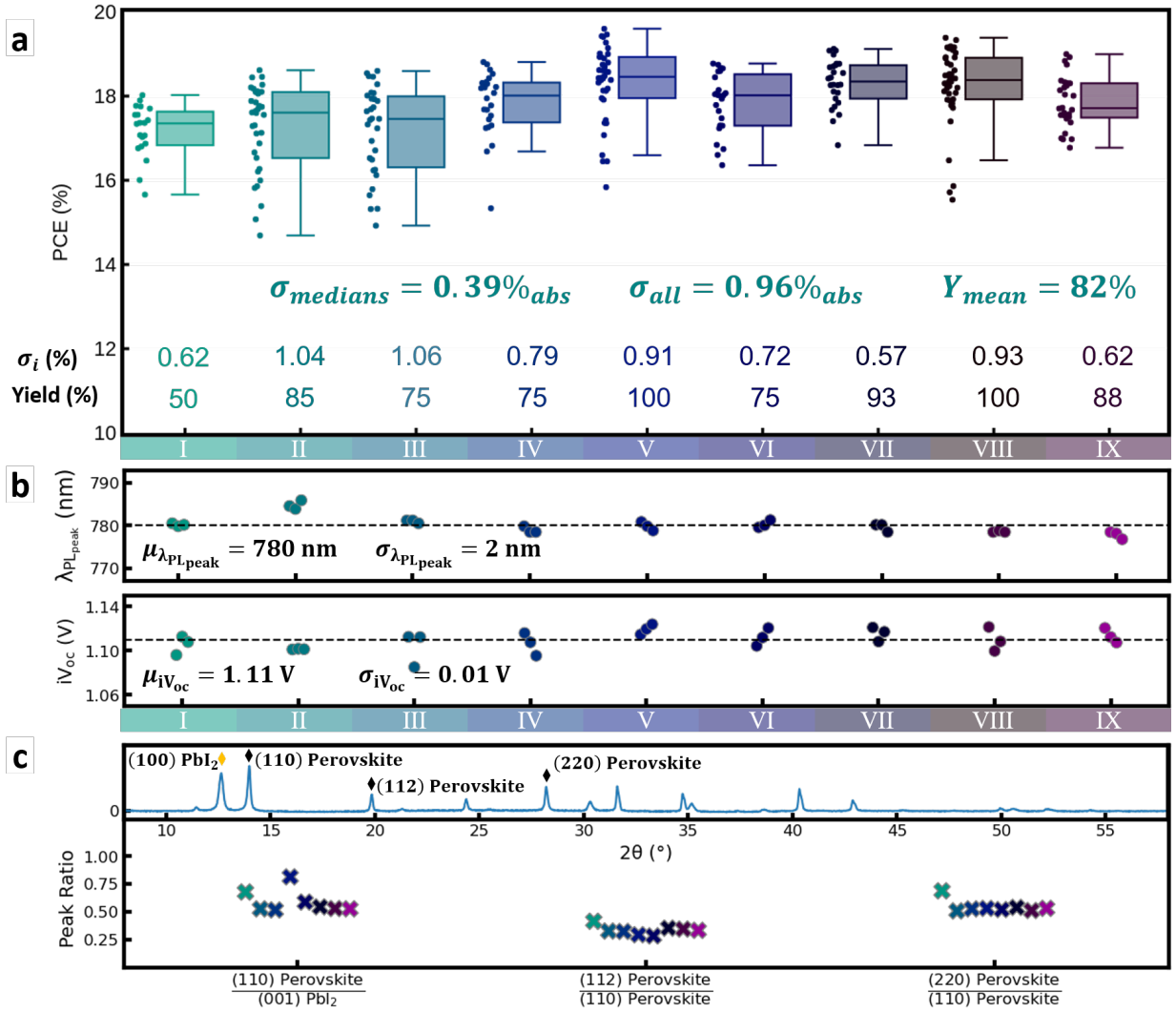

Figure 2: Performance of perovskite solar cells fabricated with our fully automated spin-coating process. a) Power conversion efficiency (PCE) statistics of nine batches with respective yields and standard deviations σ of individual batches, across all batches and of the medians. b) Photoluminescence (PL) peak wavelength $\lambda_{PL_{peak}}$ and implied open-circuit voltage (iV$_{oc}$) obtained from PL quantum yield. c) Ratio of X-ray diffraction peaks of PbI$_2$ and perovskite across the batches. The colors for the batches are the same as in the other subfigures, but batch 2 is not shown as the sample was damaged before the XRD measurement.

champion batches, disregarding the repeatability of results. The problem of repeatability and reproducibility has been previously identified in the field of perovskite photovoltaics.[4,39,40] Even within champion batches, standard deviations in PCE are often around 1 % (abs.) as seen in recent high-efficiency perovskite publications,[41–44] indicating unwarranted variability. Taking (typically not reported) non-champion batches into consideration, variability can be assumed to be much higher, implying that the variability achieved here is at least equal if not lower. A practical benefit of such low variability is its potential to be used as a benchmark reference for future experiments.

(b) Optoelectronic properties of the thin films are equally comparable across batches (see Figure 2b). The implied open circuit voltage iV_{oc} of 1.11 V — calculated from photoluminescence quantum yield (PLQY) measurements (see SI: Figure S5) — matches the V_{oc} of the devices. Furthermore, band gap determination from peak emission wavelengths of 780 ± 2 nm coincide with the inflection point of external quantum efficiency (EQE) at 1.59 eV. The peak wavelength CV of 0.25 % (rel.) is close to other reported CVs in studies that optimize film quality using photoluminescence characterizations, ranging from 0.07 % to 0.1 %.[31,45]

(c) Structural and compositional properties also suggest good repeatbility (see Figure 2c). XRD peak positions and peak ratios of the main perovskite peak compared to the PbI_2 peak are consistent. Similarly, the uniformity in the different perovskite peak ratios indicates a consistent crystallographic structure and grain orientation. The peak ratios of different perovskite and PbI_2 peaks vary only slightly (CV < 0.15) over the different batches. The ratios are obtained by comparing integrated Gaussian fits of the following XRD peaks: 13.9° (110) Perovskite, 19.8° (112) Perovskite, and 28.1° (220) Perovskite to 12.6° (001) PbI_2. The slightly higher PbI_2 peak in the XRD pattern suggests an excess of PbI_2 in the perovskite film, which can generally enhance performance by passivating defects.[46] However, excessive PbI_2 can lead to detrimental effects on long-term stability due to photodegradation.[47,48] Although long-term stability is not the focus of this study, previous studies with similar compositions have shown acceptable stability.[36] This study focuses on the repeata-

bility of the perovskite thin film formation and compared the latter to manually processed thin films, shown later, the variation of peak ratios is small.

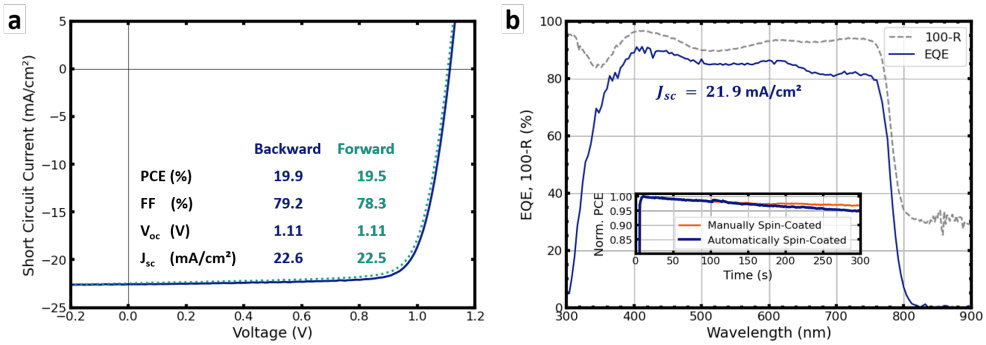

Figure 3: Champion PSC made using the fully automated perovskite spin-coating process a) current-voltage characteristics in backward and forward direction b) External quantum efficiency (EQE) of champion PSC. The inset in b shows maximum power point (MPP) tracking of the champion device and a manually processed reference cell, normalized to their respective maximum power.

Champion PSCs and transferability of established recipe: Beyond high repeatability, automated thin film fabrication can yield very high PCEs close to 20 % and is capable of adapting recipes for high-performance perovskite processing. The recipe we used (detailed in SI) has been optimized for over a decade in thousands of manually processed devices. Successful adaptation to our automated process took less than five batches, with the cells exhibiting maximum power point (MPP) behavior comparable to manually processed references.

The highest PCE for a device with an automatically fabricated perovskite thin film exceeded 19.9 %. In the current-voltage (IV) curve and characteristics (see Figure 3a), the device shows a high $FF = 79$ % and a medium $V_{oc} = 1.11$ V and $J_{sc} = 22.6$ mA/cm^2, with a minor hysteresis index of HI = 0.02. A PCE exceeding 19% was achieved in four of the nine batches. Reflection losses, limiting the quantum efficiency, have been reduced by a 125 nm MgF_2 thick anti-reflection coating (ARC). The ARC increases the J_{sc} obtained from EQE from 21.1 mA/cm^2 to 21.9 mA/cm^2 (see Figure 3b). The MPP of automatically spin-coated devices stabilizes to 18.6 % after 300 s, and behaves similarly to the manually processed

reference devices (see inset in Figure 3b). Other studies have reported champion device PCEs of 21.6 %[31] and 23.1 %[45] for perovskite thin films fully coated using automated processes. However, they used a different composition, a 2-step process under ambient conditions, and a n-i-p architecture (see SI: Table S1). In contrast, we implement the 1-step anti-solvent process in N_2 glovebox conditions for a p-i-n architecture. Compared to devices with similar layer stacks and perovskite compositions, which typically achieve PCEs of around 20 % (see SI: Table S2), our devices exhibit comparable performance.

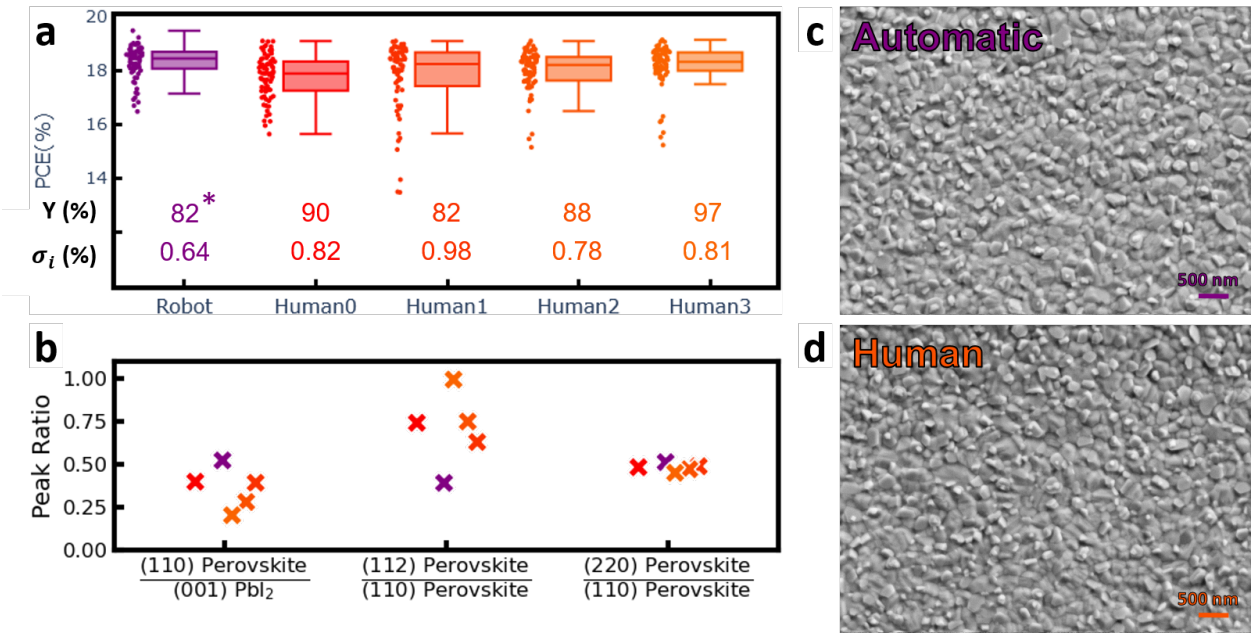

Figure 4: Comparison of automatically and manually coated perovskite thin films and device parameters a) PCE with standard deviations σ_i and yields (*not buffered by backup samples - see SI for explanation) b) XRD peak ratio of PbI_2 and perovskite c)/d) SEM images of the perovskite surface with a magnification of 20.000 show identical surface grain structure

Automated fabrication vs. human experimenter: Compared to human experimenters, our automated setup produces perovskite films of equivalent quality. We show this by systematically comparing PSCs produced by four experienced human experimenters with PSCs produced by the automated setup. Structural, compositional, and device analyses confirm the equivalent quality of the films. The previously shown repeatability that the automated setup can achieve is especially apparent when contrasted to human experimenters, all of

whom produced devices with more performance variation.

To allow for such a direct comparison (see Figure 4a), all experiments were conducted on the same day with the same precursor solution and instruments. The only varied parameter was the experimenter responsible for the spin-coating of the perovskite thin films. All human experimenters are very experienced researchers who have fabricated more than a thousand perovskite thin films and devices. An analysis of variance with a post-hoc Tukey group test (see SI) indicates no significant differences in PCE between the automatic processing and the best human experimenter. While there was no significant difference between the human experimenters, the automated setup produced significantly better thin films than two of the four experimenters. Overall, the reduced variation of the automatically processed devices compared to the manually produced devices underlines again the high process repeatability of the setup.

The grain structure exhibits consistent surface morphology between automatically and manually produced films, as revealed by scanning electron microscopy (SEM) at a magnification of 20.000 (see Figure 4c&d). The underlying grain structure consists of grains ranging from 300 to 700 nm overlaid by smaller agglomerates of only about 100 nm in diameter. These smaller agglomerates are attributed to unreacted PbI_2, of which there is a 10 % excess in the recipe by design, as they help passivate surface and grain boundary defects.[46] The comparability of the automatically and manually coated perovskite films is further supported by aligning structural and compositional properties (see Figure 4b). The XRD peak positions are consistent across the different operators. However, variations arise in peak intensities and ratios. This suggests that crystal formation and orientation are influenced by operational differences in antisolvent dispensing. The automated process achieves more consistent peak ratios across different batches (see Figure 2c).

The main advantage of automatic fabrication in comparison to manual fabrication is that all parameters for spin-coating, antisolvent dispensing, and annealing can be precisely controlled, reducing unexplained variance caused by human involvement. These parameters

include the position, height, angle, and movement of the pipette,[31] solvent dispense speed[49,50] and consistency, as well as the timing of the solvent quenching process.[51,52] This control over experimental conditions enables transfer to other systems or laboratories to collaborate, reproduce findings, and build upon them. Especially with the assistance of electronic lab notebooks[53,54] or database projects,[55] this enables efficient experimentation. In the future, this could be controlled by advanced algorithms such as Bayesian Optimizations, allowing established recipes to be transferred to the automated process and then fine-tuned. The next steps towards accelerating optimization are utilizing in-situ characterization and algorithmic decision-making for autonomous experimental planning, as recently demonstrated by Zhang et al.[31]

Comparison of homogeneity: One key asset of automated perovskite thin film processing beyond PCE, repeatability, and transferability is the enhanced homogeneity of the perovskite thin films. SEM and microscopy images show that in the center of the automatically coated films, no annular structure is present, which is commonly observed and attributed to local wrinkles in manually coated films (see Figure 5).[56,57]

The emergence of rough annular surface structures is not uncommon in manual perovskite thin film fabrication.[56,57] These micrometer-sized wrinkles (see Figure 5) are formed due to stress during the crystallization of the film.[58,59] While all manually coated films show these wrinkles, no automatically coated samples develop them. Likely, minor differences in the way the anti-solvent is dispensed onto the rotating sample cause these inhomogeneities. These differences might be due to the height and angle of holding the pipette, or due to the shape of the tip, as the robot dispenses through a syringe pump and nozzle. Neither the grain structure nor the device performance is affected by the wrinkling. It should be noted that in our layout, the active area only minimally intersects with the annular structure (see Figure S2). While it might be possible that this structure improves light in coupling, it could also be detrimental for devices with an active area in the center, by creating interfacial

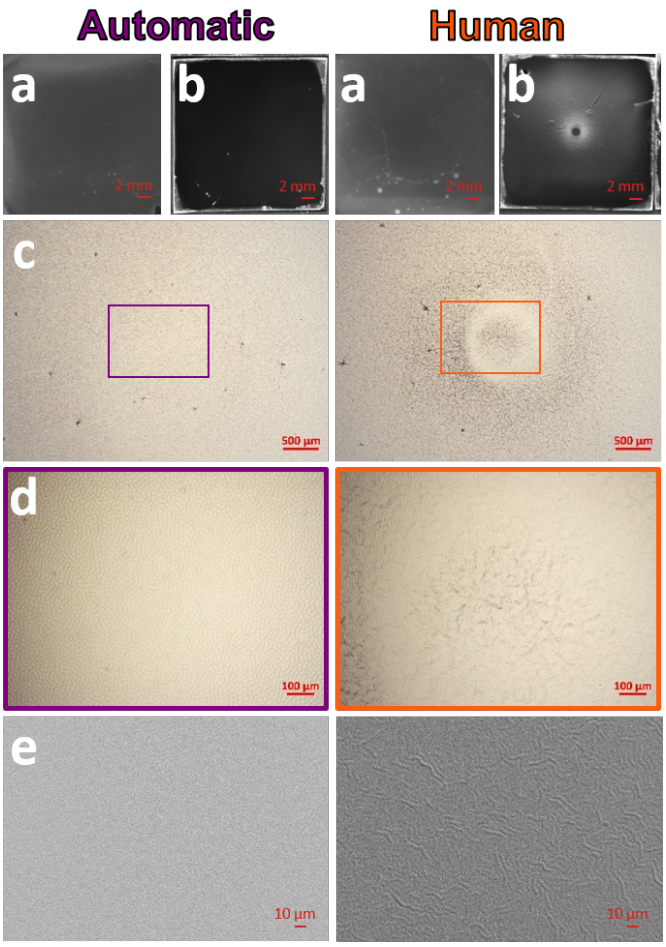

Figure 5: Improved homogeneity of automatically coated films compared to manually coated films. Representative samples show a) Spatial PL images illuminated using blue LEDs 457 nm (0.08 suns) and recorded with a camera through an optical 780 nm longpass filter, b) Diffuse reflection images with the same illumination but recorded through a neutral density filter, c/d) Optical microscope images recorded with a magnification of x5 and x20 displaying the typical wrinkles observed in the manually processes films, e) SEM images recorded under a 20keV electron beam also show these wrinkles

defects or inhomogeneous covering of subsequent layers. Other studies and reviews have shown that a homogeneous absorber is essential for realizing efficient modules in large-area devices.[60–62]

Spatial photoluminescence images reveal that homogeneity is slightly improved in automatically coated films compared to manually coated ones (see Figure 5a). While the standard deviation within the evaluated region is lower than the manual reference for half of the automatically coated films, inhomogeneities persist in the other half, yielding similar variations as the manually coated films. The evaluated region in the sample center corresponds to two-thirds of the sample width. This exclusion of the sample edges serves the purpose of excluding edge effects such as coffee ring formation.

Conclusion

This article reports on the fully automated fabrication of high-quality perovskite thin films for application in solar cells, highlighting their excellent repeatability, transferability, and homogeneity achieved through automated processing. Demonstrating consistent repeatability for nine consecutive batches, we observed minimal variations in solar cell performance, structure, composition, and optoelectronic characteristics. Notably, the champion devices achieved a PCE of 19.9 %, confirming that established perovskite recipes can be transferred to the automated process without loss of PCE. Compared to human experimenters, the automated fabrication consistently matched the performance of manually coated perovskite films, confirming the reliability and efficacy of the automated process. The thin films produced by the automatic setup exhibited improved homogeneity, eliminating annular structures that commonly arise from manual spin-coating. Importantly, this study is the first to demonstrate the anti-solvent quenching method within an N_2 glovebox using automated systems. This is particularly relevant as a majority of current high-performance perovskite PV devices reported are fabricated using quenching methods. This automatic fabrication technique

has the potential to significantly accelerate research in perovskite-based optoelectronics by providing a highly repeatable baseline process, which drives the development of standard operating procedures that can be adopted by different institutions, promoting collaboration, comparability of results, and FAIR data practices. Furthermore, the integration of this automated system with machine learning or algorithmic optimization, as demonstrated by other research groups, could lead to continuous process improvement and rapid material innovation, with applicability extending to other material science domains beyond perovskites. In conclusion, fully automated robotic spin-coating emerges as a transformative technology in perovskite solar cell research, providing a robust foundation for further experimentation and algorithmic optimization.

Experimental Materials and Methods

Solution precursors and solvents: 2PACz (TCI, CAS: 20999-38-6), Lead iodide (PbI_2, TCI, CAS: 10101-63-0) and Lead Bromide ($PbBr_2$, TCI, CAS: 10031-22-8), Formamidinium iodide (FAI, Dyenamo, CAS: 879643-71-7), Methylamonium Bromide (MABr, Greatcell Solar, CAS: 6876-37-5), Cesium Iodide (CsI, TCI, CAS: 7789-17-5), Lithium Flouride (LiF, ChemPur, CAS: 7789-24-4) Fullerene-C60 (C60, Sigma-Aldrich, CAS: 99685-96-8), Bathocuproine (BCP, Lumescence Technology, CAS: 4733-39-5), and (MgF_2, Sigma-Aldrich, CAS: 7783-40-6). Solvents including N,N-dimethylformamide $\geq$ 99.9% (DMF, CAS: 68-12-2), Dimethyl sulfoxide anhydrous $\geq$ 99.9% (DMSO, CAS: 67-68-5), and Chloro Benzene anhydrous 99.8% (CB, CAS: 108-90-7) were ordered from Sigma-Aldrich. Ethanol absolute 99.8% was ordered from VWR Chemicals.

Fabrication of perovskite solar cells: ITO substrates (sheet resistance $15\Omega/square$, Luminescence Technology, CAS: 50926-11-9) were cut in 16 mm $\times$ 16 mm and cleaned with acetone and isopropanol in an ultrasonic bath for 10 min each. The substrates were further treated with oxygen plasma for 5 min. As HTL, a monolayer of 2PACz was deposited on the

ITO substrates by spin-coating at 3000 rpm for 30 s and subsequently annealed at 100 °C for 10 min in a N_2 atmosphere. The 2PACz precursor solution was prepared by dissolving 2PACz in anhydrous ethanol with a concentration of 1.5 mM. The prepared solution was put in an ultrasonic bath for 20 min before it was used. The perovskite precursor solution was prepared by first dissolving PbI_2 (1.3 M, 602.5 mg) in a mixture of DMF:DMSO (4:1 v/v, 800 μL : 200 μL). The PbI_2 solution was kept on a hotplate at 130 °C for 15 min and added to a mixture of $PbBr_2$ (0.14 M, 51,75 mg), MABr (0.14 M, 15,8 mg) and FAI (1.2 M, 206 mg). The solution is then stirred until fully dissolved. From a CsI (1.5 M, 390 mg) in DMSO (1 mL) solution, the Csl (0.07 M, $46,7\mu$L) is added to the solution resulting in a composition described by $Cs_{0.05}MA_{0.1}FA_{0.85}Pb(I_{0.9}Br_{0.1})_3$. To spin-coat the perovskite films 100μL of the precursor solution is dispensed on the substrates, which are then spun at 1000 rpm (500 rpm s–1) for 10 s and 5000 rpm (2000 rpm s–1) for 20 s. 25 s after the start, CB (150 μL) was dispensed onto the center of the spinning substrate, at a rate of 150 $\frac{\mu L}{s}$ from 25 mm above the sample. The spin-coating is performed in a N_2 atmosphere. The samples were then annealed at 140 °C for 10 min in a nitrogen atmosphere. The passivation layer of 1 nm LiF was thermally evaporated at a rate of 0.2 Å/s. The electron transport layer, 20 nm of C60 and 3.5 nm BCP, was thermally evaporated at a rate of 0.2 Å/s while maintaining a pressure not higher than 10^{-6} mbar. Finally, 100 nm of Ag was thermally evaporated using a shadow mask with an active area of 10.5 mm^2 to complete the perovskite solar cells with 4 pixels per substrate. A 125 nm thermally evaporated at 1 Å/s MgF_2 layer as ARC was added on the glass side for the champion devices.

Characterisation of perovskite thin films and respective solar cell devices: To measure the current voltage characteristics of the solar cell devices an Oriel Sol3A Class AAA Solar Simulator, calibrated to 1 sun (±1%) intensity using a certified MKS Instruments silicon reference cell with a KG5 filter. The solar cells are measured in N_2 atmosphere and are kept at 25°C using a Peltier, thermocouple, and temperature controller. The IV

curve of the PSCs was measured in backwards and forward direction with a 10 mV step size using a Keithley 2400 source meter unit. MPP tracking was performed using a perturb and observe method.

The PLQY measurements were conducted using the LuQY Pro system of QYB. This system is equipped with an internal integrating sphere and an exciting laser with 532 nm (1 sun equivalent intensity). The iV_{oc} was calculated using the $iV_{oc} = k_B \cdot T \cdot \log(PLQY \cdot J_{sc}/J_{BB})$. The J_{sc} was derived from the EQE measurements and J_{BB} was obtained by integrating the multiplication of the EQE spectrum with the black body spectrum at T = 300 K. The photoluminescence spectra are shown in the SI (Figure S5).

The crystal structure of the perovskite layers was analysed out utilizing XRD (Bruker D2Phaser system) with Cu-Kα radiation (λ = 1.5405 Å) in Bragg–Brentano configuration using a LynxEye detector. The XRD was taken from the perovskite layer deposited on the ITO/2PAcz substrate to obtain the same perovskite nucleation as well as crystallization as in the solar cells.

The EQE was measured using a PVE300 photovoltaic QE system (Bentham EQE system). A chopping frequency of $\tilde{5}$70 Hz with an integration time of 500 ms to acquire the spectra in a wavelength range from 300 to 900 nm and a spot size of 0.74 mm^2 was used.

Reflectance spectra of the PSCs were measured using a PerkinElmer Lambda1050 spectrophotometry setup equipped with a double-monochromator and a modulated source. A chopper frequency of 46 Hz was applied.

Scanning electron microscopy (SEM) was measured out in an SEM (Zeiss LEO1530) with an aperture size of 20–30 μm. The acceleration voltages for the analysis ranged between 2 and 10 kV.

The optical microscope images were taken with a Zeiss Axioplan 2 imaging.

Supporting Information Available

In the supporting information, we show two tables containing the composition, layer stack and PCE of other automatically fabricated PSCs (SI Table S1) and of PSCs with a similar composition and layer stack (SI Table S2). We show an evolution of PSC record PCE evolution compared to all PSCs listen in the perovskite database (Figure S1). The active areas of our devices are compared to the annular structures (Figure S2). The IV Parameters for the nine consecutive batches (Figure S3) and the unfiltered device PCE (Figure S4) are shown. The PL spectra (Figure S5) and XRD spectra (Figure S6) for the nine batches are shown and the XRD spectra for the robotic - human comparison (Figure S7). Preliminary results of a Gas-quenched process are shown (Figure S8). A detailed descriptions on the yield considerations and the results of the ANOVA complete the SI.

Acknowledgement

Financial support by the Initiating and Networking funding of the Helmholtz Association (the Solar Technology Acceleration Platform (Solar TAP)), the program-oriented funding IV of the Helmholtz Association (Materials and Technologies for the Energy Transition, Topic 1: Photovoltaics and Wind Energy, Code: 38.01.04). We acknowledge support by the Karlsruhe School of Optics and Photonics (KSOP) and the Ministry of Science, Research and Arts of Baden-Württemberg as part of the sustainability financing of the projects of the Excellence Initiative II. The authors also gratefully acknowledge support from KSOP through a PhD scholarship. A warm thank you also to the whole "perovskite task force" at KIT for fruitful discussions and assistance.

We acknowledge the use of generative AI in assisting the refinement of sentence structure, grammar, and spelling, thereby contributing to the enhancement of this manuscript.

References

(1) Saliba, M.; Correa-Baena, J.-P.; Wolff, C. M.; Stolterfoht, M.; Phung, N.; Albrecht, S.; Neher, D.; Abate, A. How to Make over 20% Efficient Perovskite Solar Cells in Regular (n–i–p) and Inverted (p–i–n) Architectures. *Chemistry of Materials* **2018**, *30*, 4193–4201.

(2) Plesser, H. E. Reproducibility vs. Replicability: A Brief History of a Confused Terminology. *Frontiers in Neuroinformatics* **2018**, *11:76*.

(3) Miller, J.; Miller, J. C. *Statistics and Chemometrics for Analytical Chemistry*; Pearson education, 2018.

(4) Goetz, K. P.; Vaynzof, Y. The Challenge of Making the Same Device Twice in Perovskite Photovoltaics. *ACS Energy Letters* **2022**, *7*, 1750–1757.

(5) Xiao, Z.; Xiao, Z.; Dong, Q.; Dong, Q.; Bi, C.; Bi, C.; Shao, Y.; Shao, Y.; Yuan, Y.; Yuan, Y.; Huang, J.; Huang, J. Solvent Annealing of Perovskite-Induced Crystal Growth for Photovoltaic-Device Efficiency Enhancement. *Advanced Materials* **2014**,

(6) Cao, X.; Zhi, L.; Jia, Y.; Li, Y.; Zhao, K.; Cui, X.; Ci, L.; Zhuang, D.; Wei, J. A Review of the Role of Solvents in Formation of High-Quality Solution-Processed Perovskite Films. *ACS Applied Materials & Interfaces* **2019**, *11*, 7639–7654.

(7) Jeon, N. J.; Jeon, N. J.; Noh, J. H.; Noh, J. H.; Kim, Y. C.; Kim, Y. C.; Yang, W. S.; Yang, W. S.; Ryu, S.; Ryu, S.; Seok, S. I.; Seok, S. I. Solvent Engineering for High-Performance Inorganic–Organic Hybrid Perovskite Solar Cells. *Nature Materials* **2014**,

(8) Cakan, D. N.; Kumar, R. E.; Oberholtz, E.; Kodur, M.; Palmer, J. R.; Gupta, A.; Kaushal, K.; Vossler, H. M.; Fenning, D. P. PASCAL: The Perovskite Automated Spin Coat Assembly Line Accelerates Composition Screening in Triple-Halide Perovskite Alloys. *Digital Discovery* **2024**, *3*, 1236–1246.

(9) Sun, S.; Hartono, N. T.; Ren, Z. D.; Oviedo, F.; Buscemi, A. M.; Layurova, M.; Chen, D. X.; Ogunfunmi, T.; Thapa, J.; Ramasamy, S.; Settens, C.; DeCost, B. L.; Kusne, A. G.; Liu, Z.; Tian, S. I.; Peters, I. M.; Correa-Baena, J.-P.; Buonassisi, T. Accelerated Development of Perovskite-Inspired Materials via High-Throughput Synthesis and Machine-Learning Diagnosis. *Joule* **2019**, *3*, 1437–1451.

(10) Kirman, J.; Johnston, A.; Kuntz, D. A.; Askerka, M.; Gao, Y.; Todorović, P.; Ma, D.; Privé, G. G.; Sargent, E. H. Machine-Learning-Accelerated Perovskite Crystallization. *Matter* **2020**, *2*, 938–947.

(11) Li, Z.; Najeeb, M. A.; Alves, L.; Sherman, A. Z.; Shekar, V.; Cruz Parrilla, P.; Pendleton, I. M.; Wang, W.; Nega, P. W.; Zeller, M.; Schrier, J.; Norquist, A. J.; Chan, E. M. Robot-Accelerated Perovskite Investigation and Discovery. *Chemistry of Materials* **2020**, *32*, 5650–5663.

(12) Gu, E.; Tang, X.; Langner, S.; Duchstein, P.; Zhao, Y.; Levchuk, I.; Kalancha, V.; Stubhan, T.; Hauch, J.; Egelhaaf, H. J.; Zahn, D.; Osvet, A.; Brabec, C. J. Robot-Based High-Throughput Screening of Antisolvents for Lead Halide Perovskites. *Joule* **2020**, *4*, 1806–1822.

(13) Yang, J.; Lawrie, B. J.; Kalinin, S. V.; Ahmadi, M. High-Throughput Automated Exploration of Phase Growth Behaviors in Quasi-2D Formamidinium Metal Halide Perovskites. *Advanced Energy Materials* **2023**, *13*, 2302337.

(14) Wu, J.; Zhang, J.; Hu, M.; Reiser, P.; Torresi, L.; Friederich, P.; Lahn, L.; Kasian, O.; Guldi, D. M.; Pérez-Ojeda, M. E.; Barabash, A.; Rocha-Ortiz, J. S.; Zhao, Y.; Xie, Z.; Luo, J.; Wang, Y.; Seok, S. I.; Hauch, J. A.; Brabec, C. J. Integrated System Built for Small-Molecule Semiconductors via High-Throughput Approaches. *Journal of the American Chemical Society* **2023**, *145*, 16517–16525.

(15) Wang, T.; Li, R.; Ardekani, H.; Serrano-Luján, L.; Wang, J.; Ramezani, M.; Wilming-

ton, R.; Chauhan, M.; Epps, R. W.; Darabi, K.; Guo, B.; Sun, D.; Abolhasani, M.; Gundogdu, K.; Amassian, A. Sustainable Materials Acceleration Platform Reveals Stable and Efficient Wide-Bandgap Metal Halide Perovskite Alloys. *Matter* **2023**, *6*, 2963–2986.

(16) Moradi, S.; Kundu, S.; Awais, M.; Haruta, Y.; Nguyen, H.; Zhang, D.; Tan, F.; Saidaminov, M. I. High-Throughput Exploration of Triple-Cation Perovskites via All-in-One Compositionally-Graded Films. *Small* **2023**, *19*, 2301037.

(17) Zhang, Y.; Zhou, Y. High-Throughput Multi-Scale Experiments to Probe the Stability of Metal Halide Perovskites. *ACS Energy Letters* **2024**, *9*, 186–190.

(18) Chen, S.; Hou, Y.; Chen, H.; Tang, X.; Langner, S.; Li, N.; Stubhan, T.; Levchuk, I.; Gu, E.; Osvet, A.; Brabec, C. J. Exploring the Stability of Novel Wide Bandgap Perovskites by a Robot Based High Throughput Approach. *Advanced Energy Materials* **2017**, *8*, 1701543.

(19) Higgins, K.; Valleti, S. M.; Ziatdinov, M.; Kalinin, S. V.; Ahmadi, M. Chemical Robotics Enabled Exploration of Stability in Multicomponent Lead Halide Perovskites via Machine Learning. *ACS Energy Letters* **2020**, *5*, 3426–3436.

(20) Higgins, K.; Ziatdinov, M.; Kalinin, S. V.; Ahmadi, M. High-Throughput Study of Antisolvents on the Stability of Multicomponent Metal Halide Perovskites through Robotics-Based Synthesis and Machine Learning Approaches. *Journal of the American Chemical Society* **2021**, *143*, 19945–19955, PMID: 34793161.

(21) Zhao, Y.; Zhang, J.; Xu, Z.; Sun, S.; Langner, S.; Hartono, N. T. P.; Heumueller, T.; Hou, Y.; Elia, J.; Li, N.; Matt, G. J.; Du, X.; Meng, W.; Osvet, A.; Zhang, K.; Stubhan, T.; Feng, Y.; Hauch, J.; Sargent, E. H.; Buonassisi, T.; Brabec, C. J. Discovery of Temperature-Induced Stability Reversal in Perovskites Using High-Throughput Robotic Learning. *Nature Communications* **2021**, *12*, 2191.

(22) Zhang, J.; Langner, S.; Wu, J.; Kupfer, C.; Lüer, L.; Meng, W.; Zhao, B.; Liu, C.; Daum, M.; Osvet, A.; Li, N.; Halik, M.; Stubhan, T.; Zhao, Y.; Hauch, J. A.; Brabec, C. J. Intercalating-Organic-Cation-Induced Stability Bowing in Quasi-2D Metal-Halide Perovskites. *ACS Energy Letters* **2021**, *7*, 70–77.

(23) Zhang, J.; Wu, J.; Langner, S.; Zhao, B.; Xie, Z.; Hauch, J. A.; Afify, H. A.; Barabash, A.; Luo, J.; Sytnyk, M.; Meng, W.; Zhang, K.; Liu, C.; Osvet, A.; Li, N.; Halik, M.; Heiss, W.; Zhao, Y.; Brabec, C. J. Exploring the Steric Hindrance of Alkylammonium Cations in the Structural Reconfiguration of Quasi-2D Perovskite Materials Using a High-throughput Experimental Platform. *Advanced Functional Materials* **2022**, *32*, 2207101.

(24) Tang, Y.; Li, Z.; Nellikkal, M. A. N.; Eramian, H.; Chan, E. M.; Norquist, A. J.; Hsu, D. F.; Schrier, J. Improving Data and Prediction Quality of High-Throughput Perovskite Synthesis with Model Fusion. *Journal of Chemical Information and Modeling* **2021**, *61*, 1593–1602, PMID: 33797887.

(25) Shekar, V.; Nicholas, G.; Najeeb, M. A.; Zeile, M.; Yu, V.; Wang, X.; Slack, D.; Li, Z.; Nega, P. W.; Chan, E. M.; Norquist, A. J.; Schrier, J.; Friedler, S. A. Active Meta-Learning for Predicting and Selecting Perovskite Crystallization Experiments. *The Journal of Chemical Physics* **2022**, *156*, 064108.

(26) Lin, J.; Mo, F. Empowering Research in Chemistry and Materials Science through Intelligent Algorithms. *Artificial Intelligence Chemistry* **2024**, *2*, 100035.

(27) Amassian, A. Accelerating Hybrid Perovskite Research Through Robotic Micro-Experimentation. Organic and Hybrid Light Emitting Materials and Devices XXV. 2021; p 1180819.

(28) Du, X.; Lüer, L.; Heumueller, T.; Wagner, J.; Berger, C.; Osterrieder, T.; Wortmann, J.; Langner, S.; Vongsaysy, U.; Bertrand, M.; Li, N.; Stubhan, T.; Hauch, J.; Brabec, C. J.

Elucidating the Full Potential of OPV Materials Utilizing a High-Throughput Robot-Based Platform and Machine Learning. *Joule* **2021**, *5*, 495–506.

(29) Liu, Z.; Rolston, N.; Flick, A. C.; Colburn, T. W.; Ren, Z.; Dauskardt, R. H.; Buonassisi, T. Machine Learning with Knowledge Constraints for Process Optimization of Open-Air Perovskite Solar Cell Manufacturing. *Joule* **2022**, *6*, 834–849.

(30) Osterrieder, T.; Schmitt, F.; Lüer, L.; Wagner, J.; Heumüller, T.; Hauch, J.; Brabec, C. J. Autonomous Optimization of an Organic Solar Cell in a 4-Dimensional Parameter Space. *Energy & Environmental Science* **2023**, *16*, 3984–3993.

(31) Zhang, J.; Liu, B.; Liu, Z.; Wu, J.; Arnold, S.; Shi, H.; Osterrieder, T.; Hauch, J. A.; Wu, Z.; Luo, J.; Wagner, J.; Berger, C. G.; Stubhan, T.; Schmitt, F.; Zhang, K.; Sytnyk, M.; Heumueller, T.; Sutter-Fella, C. M.; Peters, I. M.; Zhao, Y.; Brabec, C. J. Optimizing Perovskite Thin-Film Parameter Spaces with Machine Learning-Guided Robotic Platform for High-Performance Perovskite Solar Cells. *Advanced Energy Materials* **2023**, *13*, 2302594.

(32) Ahmadi, M.; Ziatdinov, M.; Zhou, Y.; Lass, E. A.; Kalinin, S. V. Machine Learning for High-Throughput Experimental Exploration of Metal Halide Perovskites. *Joule* **2021**, *5*, 2797–2822.

(33) MacLeod, B. P.; Parlane, F. G. L.; Morrissey, T. D.; Häse, F.; Roch, L. M.; Dettelbach, K. E.; Moreira, R.; Yunker, L. P. E.; Rooney, M. B.; Deeth, J. R.; Lai, V.; Ng, G. J.; Situ, H.; Zhang, R. H.; Elliott, M. S.; Haley, T. H.; Dvorak, D. J.; Aspuru-Guzik, A.; Hein, J. E.; Berlinguette, C. P. Self-Driving Laboratory for Accelerated Discovery of Thin-Film Materials. *Science Advances* **2020**, *6*, eaaz8867.

(34) Li, J.; Lu, Y.; Xu, Y.; Liu, C.; Tu, Y.; Ye, S.; Liu, H.; Xie, Y.; Qian, H.; Zhu, X. AIR-Chem: Authentic Intelligent Robotics for Chemistry. *The Journal of Physical Chemistry A* **2018**, *122*, 9142–9148, PMID: 30395457.

(35) Burger, B.; Maffettone, P. M.; Gusev, V. V.; Aitchison, C. M.; Bai, Y.; Wang, X.; Li, X.; Alston, B. M.; Li, B.; Clowes, R.; Rankin, N.; Harris, B.; Sprick, R. S.; Cooper, A. I. A Mobile Robotic Chemist. *Nature* **2020**, *583*, 237–241.

(36) Ruiz-Preciado, M. A.; Gota, F.; Fassl, P.; Hossain, I. M.; Singh, R.; Laufer, F.; Schackmar, F.; Feeney, T.; Farag, A.; Allegro, I.; Hu, H.; Gharibzadeh, S.; Nejand, B. A.; Gevaerts, V. S.; Simor, M.; Bolt, P. J.; Paetzold, U. W. Monolithic Two-Terminal Perovskite/CIS Tandem Solar Cells with Efficiency Approaching 25%. *ACS Energy Letters* **2022**, *7*, 2273–2281.

(37) Stolterfoht, M.; Caprioglio, P.; Wolff, C. M.; Márquez, J. A.; Nordmann, J.; Zhang, S.; Rothhardt, D.; Hörmann, U.; Amir, Y.; Redinger, A.; Kegelmann, L.; Zu, F.; Albrecht, S.; Koch, N.; Kirchartz, T.; Saliba, M.; Unold, T.; Neher, D. The Impact of Energy Alignment and Interfacial Recombination on the Internal and External Open-Circuit Voltage of Perovskite Solar Cells. *Energy & Environmental Science* **2019**, *12*, 2778–2788.

(38) Hu, J.; You, J.; Peng, C.; Qiu, S.; He, W.; Li, C.; Liu, X.; Mai, Y.; Guo, F. Polyfluorene Copolymers as High-Performance Hole-Transport Materials for Inverted Perovskite Solar Cells. *Solar RRL* **2019**, *4*, 1900384.

(39) Correa-Baena, J.-P.; Saliba, M.; Buonassisi, T.; Grätzel, M.; Abate, A.; Tress, W.; Hagfeldt, A. Promises and Challenges of Perovskite Solar Cells. *Science* **2017**, *358*, 739–744.

(40) Mahapatra, A.; Kumar, S.; Kumar, P.; Pradhan, B. Recent Progress in Perovskite Solar Cells: Challenges from Efficiency to Stability. *Materials Today Chemistry* **2022**, *23*, 100686.

(41) Li, G.; Su, Z.; Canil, L.; Hughes, D.; Aldamasy, M. H.; Dagar, J.; Trofimov, S.; Wang, L.; Zuo, W.; Jerónimo-Rendon, J. J.; Byranvand, M. M.; Wang, C.; Zhu, R.;

Zhang, Z.; Yang, F.; Nasti, G.; Naydenov, B.; Tsoi, W. C.; Li, Z.; Gao, X.; Wang, Z.; Jia, Y.; Unger, E.; Saliba, M.; Li, M.; Abate, A. Highly Efficient p-i-n Perovskite Solar Cells that Endure Temperature Variations. *Science* **2023**, *379*, 399–403.

(42) Yoo, J. J.; Seo, G.; Chua, M. R.; Park, T. G.; Lu, Y.; Rotermund, F.; Kim, Y.-K.; Moon, C. S.; Jeon, N. J.; Correa-Baena, J.-P.; Bulović, V.; Shin, S. S.; Bawendi, M. G.; Seo, J. Efficient Perovskite Solar Cells via Improved Carrier Management. *Nature* **2021**, *590*, 587–593.

(43) Li, Y.; Shi, J.; Zheng, J.; Bing, J.; Yuan, J.; Cho, Y.; Tang, S.; Zhang, M.; Yao, Y.; Lau, C. F. J.; Lee, D. S.; Liao, C.; Green, M. A.; Huang, S.; Ma, W.; Ho-Baillie, A. W. Y. Acetic Acid Assisted Crystallization Strategy for High Efficiency and Long-Term Stable Perovskite Solar Cell. *Advanced Science* **2020**, *7*, 1903368.

(44) Min, H.; Kim, M.; Lee, S.-U.; Kim, H.; Kim, G.; Choi, K.; Lee, J. H.; Seok, S. I. Efficient, Stable Solar Cells by using Inherent Bandgap of α-Phase Formamidinium Lead Iodide. *Science* **2019**, *366*, 749–753.

(45) Zhang, J.; Wu, J.; Barabash, A.; Du, T.; Qiu, S.; Le Corre, V. M.; Zhao, Y.; Zhang, K.; Schmitt, F.; Peng, Z.; Tian, J.; Li, C.; Liu, C.; Heumueller, T.; Lüer, L.; Hauch, J. A.; Brabec, C. J. Precise Control of Process Parameters for $>$ 23 % Efficiency Perovskite Solar Cells in Ambient Air using an Automated Sevice Acceleration Platform. *Energy & Environmental Science* **2024**, *17*, 5490–5499.

(46) Shan, D.; Tong, G.; Cao, Y.; Tang, M.; Xu, J.; Yu, L.; Chen, K. The Effect of Decomposed PbI2 on Microscopic Mechanisms of Scattering in CH3NH3PbI3 Films. *Nanoscale Research Letters* **2019**, *14*, 208.

(47) Gao, Y.; Raza, H.; Zhang, Z.; Chen, W.; Liu, Z. Rethinking the Role of Excess/Residual Lead Iodide in Perovskite Solar Cells. *Advanced Functional Materials* **2023**, *33*, 2215171.

(48) Tumen-Ulzii, G.; Qin, C.; Klotz, D.; Leyden, M. R.; Wang, P.; Auffray, M.; Fujihara, T.; Matsushima, T.; Lee, J.; Lee, S.; Yang, Y.; Adachi, C. Detrimental Effect of Unreacted PbI2 on the Long-Term Stability of Perovskite Solar Cells. *Advanced Materials* **2020**, *32*, 1905035.

(49) Taylor, A. D.; Sun, Q.; Goetz, K. P.; An, Q.; Schramm, T.; Hofstetter, Y.; Litterst, M.; Paulus, F.; Vaynzof, Y. A General Approach to High-Efficiency Perovskite Solar Cells by any Antisolvent. *Nature Communications* **2021**, *12*, 1878.

(50) Song, T.-B.; Yuan, Z.; Babbe, F.; Nenon, D. P.; Aydin, E.; De Wolf, S.; Sutter-Fella, C. M. Dynamics of Antisolvent Processed Hybrid Metal Halide Perovskites Studied by In Situ Photoluminescence and Its Influence on Optoelectronic Properties. *ACS Applied Energy Materials* **2020**, *3*, 2386–2393.

(51) Zhao, P.; Kim, B. J.; Ren, X.; Lee, D. G.; Bang, G. J.; Jeon, J. B.; Kim, W. B.; Jung, H. S. Antisolvent with an Ultrawide Processing Window for the One-Step Fabrication of Efficient and Large-Area Perovskite Solar Cells. *Advanced Materials* **2018**, *30*, 1802763.

(52) Farag, A.; Fassl, P.; Hu, H.; Feeney, T.; Quintilla, A.; Ruiz-Preciado, M. A.; Hempel, W.; Bagrowski, D.; Noack, P.; Wattenberg, B.; Dippell, T.; Paetzold, U. W. Mitigation of Open-Circuit Voltage Losses in Perovskite Solar Cells Processed over Micrometer-Sized-Textured Si Substrates. *Advanced Functional Materials* **2022**, *33*, 2210758.

(53) Scheidgen, M.; Himanen, L.; Ladines, A. N.; Sikter, D.; Nakhaee, M.; Fekete, A.; Chang, T.; Golparvar, A.; Márquez, J. A.; Brockhauser, S.; Brückner, S.; Ghiringhelli, L. M.; Dietrich, F.; Lehmberg, D.; Denell, T.; Albino, A.; Näsström, H.; Shabih, S.; Dobener, F.; Kühbach, M.; Mozumder, R.; Rudzinski, J. F.; Daelman, N.; Pizarro, J. M.; Kuban, M.; Salazar, C.; Ondračka, P.; Bungartz, H.-J.; Draxl, C. NO-

MAD: A Distributed Web-Based Platform for Managing Materials Science Research Data. *Journal of Open Source Software* **2023**, *8*, 5388.

(54) Draxl, C.; Scheffler, M. The NOMAD Laboratory: From Data Sharing to Artificial Intelligence. *Journal of Physics: Materials* **2019**, *2*, 036001.

(55) Jacobsson, T. J.; Hultqvist, A.; García-Fernández, A.; Anand, A.; Al-Ashouri, A.; Hagfeldt, A.; Crovetto, A.; Abate, A.; Ricciardulli, A. G.; Vijayan, A.; Kulkarni, A.; Anderson, A. Y.; Darwich, B. P.; Yang, B.; Coles, B. L.; Perini, C. A. R.; Rehermann, C.; Ramirez, D.; Fairen-Jimenez, D.; Di Girolamo, D.; Jia, D.; Avila, E.; Juarez-Perez, E. J.; Baumann, F.; Mathies, F.; González, G. S. A.; Boschloo, G.; Nasti, G.; Paramasivam, G.; Martínez-Denegri, G.; Näsström, H.; Michaels, H.; Köbler, H.; Wu, H.; Benesperi, I.; Dar, M. I.; Bayrak Pehlivan, I.; Gould, I. E.; Vagott, J. N.; Dagar, J.; Kettle, J.; Yang, J.; Li, J.; Smith, J. A.; Pascual, J.; Jerónimo-Rendón, J. J.; Montoya, J. F.; Correa-Baena, J.-P.; Qiu, J.; Wang, J.; Sveinbjörnsson, K.; Hirselandt, K.; Dey, K.; Frohna, K.; Mathies, L.; Castriotta, L. A.; Aldamasy, M. H.; Vasquez-Montoya, M.; Ruiz-Preciado, M. A.; Flatken, M. A.; Khenkin, M. V.; Grischek, M.; Kedia, M.; Saliba, M.; Anaya, M.; Veldhoen, M.; Arora, N.; Shargaieva, O.; Maus, O.; Game, O. S.; Yudilevich, O.; Fassl, P.; Zhou, Q.; Betancur, R.; Munir, R.; Patidar, R.; Stranks, S. D.; Alam, S.; Kar, S.; Unold, T.; Abzieher, T.; Edvinsson, T.; David, T. W.; Paetzold, U. W.; Zia, W.; Fu, W.; Zuo, W.; Schröder, V. R. F.; Tress, W.; Zhang, X.; Chiang, Y.-H.; Iqbal, Z.; Xie, Z.; Unger, E. An Open-Access Database and Analysis Tool for Perovskite Solar Cells Based on the FAIR Data Principles. *Nature Energy* **2021**, *7*, 107–115.

(56) Braunger, S.; Mundt, L. E.; Wolff, C. M.; Mews, M.; Rehermann, C.; Jošt, M.; Tejada, A.; Eisenhauer, D.; Becker, C.; Guerra, J. A.; Unger, E.; Korte, L.; Neher, D.; Schubert, M. C.; Rech, B.; Albrecht, S. CsxFA1–xPb(I1–yBry)3 Perovskite Composi-

tions: the Appearance of Wrinkled Morphology and its Impact on Solar Cell Performance. *The Journal of Physical Chemistry C* **2018**, *122*, 17123–17135.

(57) Tejada, A.; Braunger, S.; Korte, L.; Albrecht, S.; Rech, B.; Guerra, J. A. Optical Characterization and Bandgap Engineering of Flat and Wrinkle-Textured FA0.83Cs0.17Pb(I1–xBrx)3 Perovskite Thin Films. *Journal of Applied Physics* **2018**, *123*, 175302.

(58) Bush, K. A.; Rolston, N.; Gold-Parker, A.; Manzoor, S.; Hausele, J.; Yu, Z. J.; Raiford, J. A.; Cheacharoen, R.; Holman, Z. C.; Toney, M. F.; Dauskardt, R. H.; McGehee, M. D. Controlling Thin-Film Stress and Wrinkling during Perovskite Film Formation. *ACS Energy Letters* **2018**, *3*, 1225–1232.

(59) Guo, B.; Chauhan, M.; Woodward, N. R.; McAndrews, G. R.; Thapa, G. J.; Lefler, B. M.; Li, R.; Wang, T.; Darabi, K.; McGehee, M. D.; Amassian, A. In situ Stress Monitoring Reveals Tension and Wrinkling Evolutions during Halide Perovskite Film Formation. *ACS Energy Letters* **2024**, *9*, 75–84.

(60) Dasgupta, A.; Mahesh, S.; Caprioglio, P.; Lin, Y.-H.; Zaininger, K.-A.; Oliver, R. D.; Holzhey, P.; Zhou, S.; McCarthy, M. M.; Smith, J. A.; Frenzel, M.; Christoforo, M. G.; Ball, J. M.; Wenger, B.; Snaith, H. J. Visualizing Macroscopic Inhomogeneities in Perovskite Solar Cells. *ACS Energy Letters* **2022**, *7*, 2311–2322.

(61) Yang, C.; Zhi, R.; Rothmann, M. U.; Huang, F.; Cheng, Y.-B.; Li, W. Toward Commercialization of Efficient and Stable Perovskite Solar Modules. *Solar RRL* **2021**, *6*, 2100600.

(62) Lee, D.-K.; Park, N.-G. Materials and Methods for High-Efficiency Perovskite Solar Modules. *Solar RRL* **2021**, *6*, 2100455.

TOC Graphic

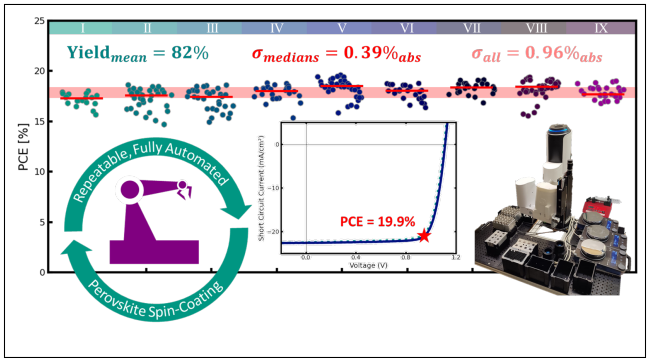
I
II
III
IV
V
VI
VII
VIII
IX
Yield$_{mean}$ = 82%
$\sigma_{medians}$ = 0.39%$_{abs}$
σ_{all} = 0.96%$_{abs}$
PCE [%]
25
20
15
10
5
0
Repeatable, Fully Automated
Perovskite Spin-Coating
PCE = 19.9%
Short Circuit Current (mA/cm²)
Voltage (V)